ORIGINAL PAPER

Structural evolution of a $2M_1$ phengite mica up to 11 GPa: an in situ single-crystal X-ray diffraction study

G. Diego Gatta · Nicola Rotiroti · Paolo Lotti · Alessandro Pavese · Nadia Curetti

Abstract The structural evolution at high pressure of a natural $2M_1$-phengite [$(K_{0.98}Na_{0.02})_{\Sigma=1.00}(Al_{1.55}Mg_{0.24}Fe_{0.21}Ti_{0.02})_{\Sigma=2.01}(Si_{3.38}Al_{0.62})O_{10}(OH)_2$; $a = 5.228(2)$, $b = 9.057(3)$, $c = 19.971(6)$Å, $\beta = 95.76(2)°$; space group: $C2/c$] from the metamorphic complex of Cima Pal (Sesia Zone, Western Alps, Italy) was studied by single-crystal X-ray diffraction with a diamond anvil cell under hydrostatic conditions up to ~ 11 GPa. A series of 12 structure refinements were performed at selected pressures within the P range investigated. The compressional behaviour of the same phengite sample was previously studied up to ~ 25 GPa by synchrotron X-ray powder diffraction, showing an irreversible transformation with a drastic decrease of the crystallinity at $P > 15–17$ GPa. The elastic behaviour between 0.0001 and 17 GPa was modelled by a third-order Birch–Murnaghan Equation of State (BM-EoS), yielding to $K_{T0} = 57.3(10)$ GPa and $K' = \partial K_{T0}/\partial P = 6.97(24)$. The single-crystal structure refinements showed that the significant elastic anisotropy of the $2M_1$-phengite (with $\beta(a):\beta(b):\beta(c) = 1:1.17:4.60$) is mainly controlled by the anisotropic compression of the K-polyhedra. The evolution of the volume of the inter-layer K-polyhedron as a function of P shows a negative slope, Fitting the $P–V$(K-polyhedron) data with a truncated second-order BM-EoS we obtain a bulk modulus value of K_{T0}(K-polyhedron) $= 26(1)$ GPa. Tetrahedra and octahedra are significantly stiffer than the K-polyhedron. Tetrahedra behave as quasi-rigid units within the P range investigated. In contrast, a monotonic decrease is observed for the octahedron volume, with $K_{T0} = 120(10)$ GPa derived by a BM-EoS. The anisotropic response to pressure of the K-polyhedron affects the P-induced deformation mechanism on the tetrahedral sheet, consisting in a cooperative rotation of the tetrahedra and producing a significant ditrigonalization of the six-membered rings. The volume of the K-polyhedron and the value of the ditrigonal rotation parameter (α) show a high negative correlation (about 93%), though a slight discontinuity is observed at $P > 8$ GPa. α increases linearly with P up to 7–8 GPa (with $\partial\alpha/\partial P \approx 0.7°$/GPa), whereas at higher Ps a "saturation plateau" is visible. A comparison between the main deformation mechanisms as a function of pressure observed in $2M_1$- and $3T$-phengite is discussed.

Keywords Mica · Phengite · High-pressure · Compressibility · Single-crystal X-ray diffraction

G. Diego Gatta (✉) · N. Rotiroti · P. Lotti · A. Pavese
Dipartimento di Scienze della Terra,
Università degli Studi di Milano, Via Botticelli 23,
20133 Milan, Italy
e-mail: diego.gatta@unimi.it

G. Diego Gatta · N. Rotiroti · A. Pavese
CNR, Istituto per la Dinamica dei Processi Ambientali,
Milan, Italy

N. Curetti
Dipartimento Scienze Mineralogiche e Petrologiche,
Università degli Studi di Torino, Via Valperga Caluso 35,
10125 Torino, Italy

Introduction

Phengites are dioctahedral phyllosilicates belonging to the muscovite–celadonite series, with general chemical formula $KAl_{2-y}(Fe,Mg)_y(Si_{3+y}Al_{1-y})O_{10}(OH)_2$ (ideally $y = 0.5$) (Rieder et al. 1999). In nature, phengites occur in metamorphic rocks, especially in low- and medium-pressure environments as a transformation product of clay minerals and are widely used as geo-barometer or

geo-thermometer (Guidotti and Sassi 2002 and references therein; Kisch et al. 2006). The two most common polytypes of phengite are the $2M_1$ (S.G. $C2/c$, with $a \sim 5.2$, $b \sim 9.06$, $c \sim 19.97$ Å and $\beta \sim 95.8°$) and $3T$ (S.G. $P3_112$, with $a = b \sim 5.2$ and $c \sim 29.8$ Å). The structural relationships between the polytypes of this class of materials have been widely studied and recently reviewed (Nespolo and Ferraris 2001; Nespolo and Ďurovič 2002). The findings of several studies on the occurrence and phase-stability of phengites have led to the following general conclusions: (1) the formation of different polytypes is likely controlled by conditions and mechanisms of growth; (2) the limited variety of polytypes found in methamorphic (white) micas suggests that their formation is favoured by specific P–T conditions; (3) large P/T values seem to promote crystallisation of the trigonal polytype (Sassi et al. 1994; Guidotti and Sassi 1998; Pavese et al. 1999; Smyth et al. 2000; Guidotti and Sassi 2002; Curetti et al. 2006, 2008). Ivaldi et al. (2001), and Ferraris and Ivaldi (2002) pointed out that the high stability under non-ambient conditions of the trigonal polytype might be ascribed to some crystallographic features: (1) the $3T$-polytype having two symmetry-independent octahedral sites (against only one in $2M_1$), which allow a better arrangement of the cations in the octahedral sheet; (2) the orientation of the hydroxyl group in the trigonal polytype giving rise to an energetically more favourable configuration.

Among the rock-forming silicates, a few studies describe the elastic behaviour and P-induced structural evolution of dioctahedral micas (Vaughan and Guggenheim 1986; Sekine et al. 1991; Faust and Knittle 1994; Catti et al. 1994; Comodi and Zanazzi 1995, 1997; Pavese et al. 1999; Smyth et al. 2000; Curetti et al. 2006; Gatta et al. 2009). About phengites, the first description of the thermo-elastic behaviour of a natural $3T$-polytype by in situ synchrotron X-ray powder diffraction with a Paris–Edinburgh cell was provided by Pavese et al. (1999). Later, Smyth et al. (2000) reported the evolution of the unit-cell parameters under hydrostatic pressure of synthetic $3T$- and $2M_1$-phengite samples by HP single-crystal X-ray diffraction with a diamond anvil cell (DAC). Curetti et al. (2006) investigated the elastic properties and the stability field at high pressure of coexisting natural $3T$ and $2M_1$ phengites, with similar chemical composition, by in situ synchrotron X-ray powder diffraction with a DAC up to $P \sim 27$ GPa, using nitrogen as P-transmitting medium. At pressures above 15–17 GPa, the $2M_1$-polytype experienced an irreversible transformation with a drastic decrease of the crystallinity; whereas no evidence of anomalous elastic behaviour or phase-transition was observed for the $3T$-polytype up to 27 GPa. The authors claimed such results to be consistent with the hypothesis of stability of the $3T$-polytype in the high-pressure regime. The elastic behaviour was modelled fitting the P–V data with a

third-order Birch–Murnaghan Equation of State (BM-EoS, Angel 2000), yielding $V_0 = 703.88$ Å, $K_{T0} = 60.4(7)$ GPa and $K_0' = 5.79(11)$ for the $3T$-polytype (P range 0.0001–27 GPa), and $V_0 = 938.88$ Å, $K_{T0} = 57(1)$ GPa and $K_0' = 6.97(24)$ for the $2M_1$-polytype (P range 0.0001–17 GPa). Recently, Gatta et al. (2009) described the P-induced structural evolution of the $3T$-phengite (previously studied by Curetti et al. 2006) by in situ single-crystal X-ray diffraction with a DAC, on the basis of a series of structural refinements between 0.0001 and 10 GPa.
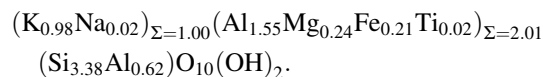
In this light, the aim of this study is

1. To investigate the P-driven structural evolution of a natural $2M_1$-phengite by single-crystal X-ray diffraction with a DAC up to 10–11 GPa;
2. To complement the previous HP-experiments that provided only unit-cell parameters at different pressures and no in situ structural refinement (Smyth et al. 2000; Curetti et al. 2006). A comparison between the main deformation mechanisms in response to pressure observed in $2M_1$- and $3T$-phengite will be here discussed.

Sample description and experimental methods

The natural $2M_1$-phengite sample here investigated has been collected in a metamorphic dike crossing eclogitic rocks and outcropping at Cima Pal (Sesia Zone, Val Savenca, Western Alps, Italy), and it is the same sample previously used by Curetti et al. (2006) for their experiments. Compagnoni (1977) reported that the rocks of the Sesia Zone experienced an eclogite-facies metamorphism at $T \sim 550°C$ and $P \sim 1.6$–1.8 GPa, with a subsequent greenschist-facies retrogression at $P \sim 0.4$–0.5 GPa and $T \sim 500°C$.

The chemical composition of the monoclinic phengite crystals used in the present study was determined by electron microprobe analyses in wavelength dispersive mode and previously reported by Ivaldi et al. (2001) and Curetti et al. (2006). The resulting chemical formula unit is

$$(K_{0.98}Na_{0.02})_{\Sigma=1.00}(Al_{1.55}Mg_{0.24}Fe_{0.21}Ti_{0.02})_{\Sigma=2.01}$$
$$(Si_{3.38}Al_{0.62})O_{10}(OH)_2.$$

One platy crystal ($180 \times 150 \times 30$ μm³), free of defects under the transmission polarised-light microscope, was selected for the X-ray diffraction experiments. Intensity diffraction data were first collected at room conditions by an Xcalibur Oxford Diffraction diffractometer equipped with a CCD, using a graphite-monochromatised MoKα-radiation and operated at 50 kV and 40 mA. A combination of ω and φ scans, with a step size of 0.4° and a time of 20 s/frame, was used to maximize the accessible reciprocal space portion and

optimize redundancy. The distance between the crystal and the detector was set to 80 mm. A total number of 10,421 Bragg reflections were collected in the range $2 < 2\theta < 70°$, of which 2,084 were unique, giving a metrically monoclinic C-centred lattice with $a = 5.228(2)$, $b = 9.057(3)$, $c = 19.971(6)$ Å and $\beta = 95.76(2)°$ (Table 1). Intensities were then corrected for Lorentz-polarization (Lp) and absorption effects; for the latter, we used the CrysAlis package (Oxford Diffraction 2008), adopting a Gaussian integration based upon the shape and dimensions of the crystal. After correction, the discrepancy factor among symmetry-related reflections (Laue class 2/m) was $R_{int} = 0.0677$ (Table 1). The reflection conditions were consistent with those of the space group $C2/c$. The anisotropic structural refinement was conducted using the SHELX-97 software (Sheldrick 1997), starting from the atomic coordinates of Ivaldi et al. (2001) and adopting a H-free structural model. Neutral atomic scattering factors of K, Al, Fe, Si and O from the International Tables for Crystallography (Wilson and Prince 1999) were used. In particular: (1) the X-ray scattering curve of potassium yielded a K-site partially empty (Table 2); (2) the Al/Fe fraction at the M-site was refined; (3) an Al–Si mixed scattering curve was used to model the two independent tetrahedral sites (i.e. T1 and T2, Table 2), though this did not improve the figures of merit of the refinement with respect to that obtained by the X-ray scattering curve of Si only. When the convergence was achieved, no residual peak larger than $+0.98/-0.77$ $e^-/Å^3$ was present in the final difference-Fourier synthesis. Despite the long exposure time per frame (Table 1), no significant electron density residue at $\pm b/3$ has been observed, suggesting a substantial absence of stacking disorder to occur (Ivaldi et al. 2001; Nespolo and Ferraris 2001). This is in keeping with that slips and stacking faults are rarer in di-octahedral than in tri-octahedral micas. Further details pertaining to the data collection protocol and structural refinements at ambient conditions are reported in Tables 1, 2 and 3.

A further data collection at room conditions was performed using a KUMA-KM4 diffractometer, equipped with a point-detector and a monochromatised Mo$K\alpha$-radiation, adopting the data collection strategy reported in Table 1. Integrated intensities were obtained using the computer software Win-IntegrSTP-3.5 (Angel 2003). Corrections for Lp and absorption have been performed using the ABSORB 5.2 computer program (Burnham 1966; Angel 2002). The anisotropic structure refinement was performed adopting the same strategy previously described. Further details about the structural refinement are set out in Tables 1, 2, and 3.

The high-pressure diffraction experiments were performed with an ETH-type diamond anvil cell, designed by Miletich et al. (2000). A foil of steel T301, 250-μm-thick,

was used as a gasket. The gasket foil (1 cm^2) was pre-indented to a thickness of about 90 μm before drilling a hole (Ø 320 μm) by spark-erosion. The same crystal of monoclinic phengite studied at ambient conditions was placed into the gasket hole for the in situ HP-experiments. A methanol:ethanol:water (16:3:1) mixture was used as a hydrostatic pressure-transmitting medium up to ~ 11 GPa (Angel et al. 2007). The pressure was determined on the basis of the third-order Birch–Murnaghan Equation-of-State reported by Curetti et al. (2006), for the same sample of natural phengite, with $K_{T0} = 57.3(10)$ GPa and $K' = \partial K_{T0}/\partial P = 6.97(24)$. Accurate unit-cell parameters at high-pressure have been measured on the basis of 32 Bragg reflections with $15 < 2\theta < 35°$. Data collections at 0.0001 GPa (crystal in DAC without any pressure medium, P0), 0.78(6) (P1), 1.76(7) (P2), 2.40(7) (P3), 3.34(6) (P4), 5.38(7) (P5, in decompression), 6.30(9) (P6), 7.13(9) (P7), 9.73(8) (P8), 9.95(9) (P9) and 11.40(10) GPa (P10) (Table 1) were performed using a KUMA-KM4 diffractometer, adopting the same experimental set-up, strategy and data treatment as those used with the crystal in air. Absorption effects due to the crystal and DAC were corrected (Burnham 1966; Angel 2002). No violation of the reflection conditions of the $C2/c$ symmetry was observed within the P range investigated.

In order to reduce the number of refined parameters, the structure refinements with the crystal in the DAC at any pressure were carried out with isotropic displacement factors (IDF), constraining all of the T-sites and all of the O-sites to share one IDF value per group, respectively (Table 2). The occupancy factors of the K-, M-, T1- and T2-site were fixed at their values determined in air. No electron density peak higher than ± 1 $e^-/Å^3$ revealed in the difference-Fourier synthesis for any explored pressure. The structural refinement based on the data collected during decompression (at ~ 5.38 GPa) showed a full reversibility of the P-induced changes, up to ~ 11 GPa and under hydrostatic conditions (Tables 1, 2, 3). After decompression to 0.0001 GPa, the unit-cell parameters measured with the crystal in air with the Xcalibur-CCD diffractometer were $a = 5.220(4)$, $b = 9.059(5)$, $c = 19.965(7)$ Å and $\beta = 95.78(4)°$.

Results: pressure-induced structural evolution

Ten structural refinements performed at different pressures between 0.0001 and 11.4 GPa allowed a full description of the main deformation mechanisms of 2M_1-phengite in response to pressure.

The elastic anisotropy observed by Curetti et al. (2006), with $\beta(a) = 0.00250(5)$, $\beta(b) = 0.00292(7)$ and $\beta(c) = 0.0115(2)$GPa^{-1} [$\beta(a):\beta(b):\beta(c) = 1:1.17:4.60$], is due to

Table 1 Details about the data collection and structural refinements at different pressures

P (GPa)	0.0001 (P$_0$-AIR)	0.0001 (P$_0$-AIR)	0.0001[a] (P$_0$)	0.78(6) (P$_1$)	1.76(7) (P$_2$)	2.40(7) (P$_3$)	3.34(6) (P$_4$)	5.38(7) (P$_5$[b])	6.30(9) (P$_6$)	7.13(9) (P$_7$)	9.73(8) (P$_8$)	9.95(9) (P$_9$)	11.40(10) (P$_{10}$)
Diffractometer	Xcalibur-CCD	Kuma-PD	Kuma-PD	Kuma-PD	Kuma-PD	Kuma-PD	Kuma-PD	Kuma-PD	Kuma-PD	Kuma-PD	Kuma-PD	Kuma-PD	Kuma-PD
X-ray radiation	Mo-$K\alpha$	Mo-$K\alpha$	Mo-$K\alpha$	Mo-$K\alpha$	Mo-$K\alpha$	Mo-$K\alpha$	Mo-$K\alpha$	Mo-$K\alpha$	Mo-$K\alpha$	Mo-$K\alpha$	Mo-$K\alpha$	Mo-$K\alpha$	Mo-$K\alpha$
Scan type	ω/φ	ω	ω	ω	ω	ω	ω	ω	ω	ω	ω	ω	ω
Scan width (°)	0.4	1.4	1.4	1.4	1.4	1.4	1.4	1.4	1.4	1.4	1.4	1.4	1.4
Scan speed (°/s)	–	0.02	0.02	0.02	0.02	0.02	0.02	0.02	0.02	0.02	0.02	0.02	0.02
Exposure (s/frame)	20	–	–	–	–	–	–	–	–	–	–	–	–
Temperature (K)	293	293	293	293	293	293	293	293	293	293	293	293	293
Space group	C 2/c	C 2/c	C 2/c	C 2/c	C 2/c	C 2/c	C 2/c	C 2/c	C 2/c	C 2/c	C 2/c	C 2/c	C 2/c
a (Å)	5.228(2)	5.218(2)	5.214(3)	5.205(2)	5.195(2)	5.183(7)	5.175(3)	5.146(2)	5.138(4)	5.128(2)	5.101(2)	5.095(3)	5.084(3)
b (Å)	9.057(3)	9.062(4)	9.058(2)	9.031(3)	9.012(3)	8.999(2)	8.969(3)	8.919(2)	8.897(3)	8.876(3)	8.824(2)	8.814(3)	8.791(3)
c (Å)	19.971(6)	19.950(5)	19.936(9)	19.804(9)	19.556(9)	19.457(9)	19.311(9)	19.027(9)	18.958(9)	18.855(9)	18.617(9)	18.606(9)	18.525(9)
β (°)	95.76(2)	95.89(6)	95.77(9)	95.84(13)	95.77(17)	95.77(17)	95.73(12)	95.74(12)	95.64(25)	95.66(13)	95.51(13)	95.52(15)	95.52(15)
V (Å³)	940.9(2)	938.4(6)	936.8(7)	926.1(6)	910.9(6)	902.9(13)	891.8(9)	868.9(6)	862.5(8)	854.0(6)	834.1(6)	831.7(7)	824.1(7)
Z	4	4	4	4	4	4	4	4	4	4	4	4	4
Maximum 2θ (°)	70.05	60.09	59.66	60.04	60.02	63.77	63.93	67.98	63.50	68.16	68.12	67.92	69.11
Measured reflections	10421	2930	356	384	374	389	387	387	388	387	361	349	580
Unique reflections	2084	1380	191	199	209	218	218	226	209	216	195	192	188
Unique reflections with $F_o > 4\sigma$ (F_o)	1115	852	167	170	168	171	183	190	161	181	161	164	168
Rint	0.0677	0.0592	0.0515	0.0613	0.0507	0.0552	0.0634	0.0626	0.0870	0.0517	0.0760	0.0788	0.0715
Number of l.s. parameters	91	91	33	33	33	33	33	33	33	33	33	33	33
R_1, $F_o > 4\sigma(F_o)$	0.0502	0.0368	0.0999	0.0962	0.0859	0.0905	0.0929	0.0972	0.0951	0.0946	0.1179	0.1312	0.1346
GoF	1.094	1.005	1.603	1.727	1.540	1.441	1.270	1.703	1.328	1.697	1.779	1.704	2.649
Residuals (e^-/Å³)	+0.98/ −0.77	+0.90/ −0.54	+0.51/ −0.66	+0.63/ −0.67	+0.55/ −0.55	+0.53/ −0.59	+0.57/ −0.56	+0.67/ −0.94	+0.55/ −0.66	+0.74/ −0.64	+0.93/ −0.81	+0.93/ −0.92	+1.09/ −0.99

Standard errors, in units of the last decimal place, are given in parentheses. A few are given to two places to avoid misunderstanding

[a] With the crystal in the DAC without P-medium

[b] In decompression

Table 2 Refined atomic positions and thermal displacement parameters (Å^2) at different pressures

Sites	P (GPa)	x	y	z	Uiso, Ueq
K (4e)	0.0001 CCD	0	0.0959(2)	1/4	0.0259(4)
	0.0001 PD	0	0.0957(2)	1/4	0.0250(4)
	P_0^a	0	0.0963(9)	1/4	0.026(2)
	P_1	0	0.095(1)	1/4	0.021(3)
	P_2	0	0.093(1)	1/4	0.023(2)
	P_3	0	0.0940(9)	1/4	0.019(2)
	P_4	0	0.0944(8)	1/4	0.017(2)
	P_5^b	0	0.0936(8)	1/4	0.015(2)
	P_6	0	0.0916(9)	1/4	0.014(2)
	P_7	0	0.0928(8)	1/4	0.015(2)
	P_8	0	0.089(1)	1/4	0.006(2)
	P_9	0	0.091(1)	1/4	0.009(2)
	P_{10}	0	0.092(1)	1/4	0.008(2)
M (8f)	0.0001 CCD	0.2469(2)	0.0824(1)	−0.00003(5)	0.0093(2)
	0.0001 PD	0.2471(2)	0.0824(1)	0.00004(5)	0.0084(3)
	P_0^a	0.247(1)	0.0826(6)	−0.0008(7)	0.007(2)
	P_1	0.246(1)	0.0822(6)	−0.0010(7)	0.005(2)
	P_2	0.247(1)	0.0840(6)	−0.0003(7)	0.008(1)
	P_3	0.246(1)	0.0821(6)	0.0001(7)	0.009(2)
	P_4	0.250(1)	0.0822(5)	0.0021(8)	0.008(1)
	P_5^b	0.245(1)	0.0818(6)	−0.0002(6)	0.005(2)
	P_6	0.248(1)	0.0822(6)	0.0005(6)	0.007(2)
	P_7	0.244(1)	0.0817(6)	−0.0001(7)	0.007(1)
	P_8	0.247(1)	0.0824(8)	−0.0013(9)	0.004(2)
	P_9	0.247(2)	0.0807(7)	0.000(1)	0.005(2)
	P_{10}	0.245(2)	0.0812(9)	−0.002(1)	0.003(2)
T1 (8f)	0.0001 CCD	0.4636(2)	0.92906(9)	0.13561(5)	0.0078(3)
	0.0001 PD	0.4637(2)	0.9291(1)	0.13551(5)	0.0072(3)
	P_0^a	0.465(1)	0.9288(5)	0.1364(8)	0.005(1)
	P_1	0.465(1)	0.9293(6)	0.1366(8)	0.001(3)
	P_2	0.468(1)	0.9268(6)	0.1378(8)	0.005(1)
	P_3	0.465(1)	0.9277(6)	0.1383(8)	0.003(1)
	P_4	0.464(1)	0.9271(5)	0.1390(8)	0.005(1)
	P_5^b	0.468(1)	0.9264(6)	0.1409(8)	0.004(1)
	P_6	0.466(1)	0.9239(8)	0.1413(8)	0.009(1)
	P_7	0.467(1)	0.9253(6)	0.1412(8)	0.005(1)
	P_8	0.466(1)	0.9248(6)	0.143(1)	0.003(2)
	P_9	0.466(1)	0.923(1)	0.144(1)	0.002(2)
	P_{10}	0.468(1)	0.925(1)	0.143(1)	0.001(2)
T2 (8f)	0.0001 CCD	0.4522(2)	0.2588(1)	0.13547(5)	0.0076(3)
	0.0001 PD	0.4523(2)	0.2587(1)	0.13563(5)	0.0064(3)
	P_0^a	0.453(1)	0.2585(6)	0.1352(8)	0.005(1)
	P_1	0.454(1)	0.2586(7)	0.1376(8)	0.003(1)
	P_2	0.454(1)	0.2569(7)	0.1370(7)	0.005(1)
	P_3	0.454(1)	0.2574(6)	0.1380(7)	0.003(1)
	P_4	0.455(1)	0.2577(6)	0.1394(7)	0.005(1)
	P_5^b	0.455(1)	0.2563(6)	0.1401(8)	0.004(1)
	P_6	0.455(1)	0.2557(7)	0.1415(9)	0.009(1)
	P_7	0.456(1)	0.2562(6)	0.1413(7)	0.005(1)
	P_8	0.459(1)	0.2565(9)	0.145(1)	0.003(2)
	P_9	0.460(1)	0.256(1)	0.144(1)	0.002(2)
	P_{10}	0.458(2)	0.255(1)	0.144(1)	0.001(2)

Table 2 continued

Sites	P (GPa)	x	y	z	Uiso, Ueq
O1 (8f)	0.0001 CCD	0.4448(5)	0.0929(3)	0.1691(1)	0.0183(5)
	0.0001 PD	0.4456(5)	0.0935(3)	0.1689(1)	0.0180(6)
	P_0^a	0.450(2)	0.094(1)	0.169(1)	0.017(2)
	P_1	0.446(2)	0.093(1)	0.171(1)	0.013(2)
	P_2	0.440(2)	0.091(1)	0.171(1)	0.016(2)
	P_3	0.441(2)	0.091(1)	0.173(1)	0.015(2)
	P_4	0.437(3)	0.091(1)	0.173(1)	0.018(2)
	P_5^b	0.428(2)	0.091(1)	0.175(1)	0.013(2)
	P_6	0.430(2)	0.088(1)	0.175(1)	0.018(2)
	P_7	0.425(2)	0.090(1)	0.177(1)	0.018(2)
	P_8	0.426(3)	0.089(2)	0.181(1)	0.010(2)
	P_9	0.423(3)	0.090(2)	0.180(1)	0.013(2)
	P_{10}	0.421(3)	0.088(2)	0.181(2)	0.013(2)
O2 (8f)	0.0001 CCD	0.2340(5)	0.8281(3)	0.1610(1)	0.0196(6)
	0.0001 PD	0.2342(5)	0.8275(3)	0.1611(1)	0.0194(7)
	P_0^a	0.235(3)	0.826(1)	0.162(1)	0.017(2)
	P_1	0.235(3)	0.826(1)	0.162(1)	0.013(2)
	P_2	0.237(3)	0.823(1)	0.164(1)	0.016(2)
	P_3	0.238(3)	0.823(1)	0.164(1)	0.015(2)
	P_4	0.245(2)	0.819(1)	0.173(1)	0.018(2)
	P_5^b	0.246(2)	0.817(1)	0.166(2)	0.013(2)
	P_6	0.244(2)	0.813(1)	0.169(2)	0.018(2)
	P_7	0.249(2)	0.811(1)	0.167(2)	0.018(2)
	P_8	0.251(3)	0.813(2)	0.175(2)	0.010(2)
	P_9	0.255(3)	0.810(2)	0.176(2)	0.013(2)
	P_{10}	0.255(3)	0.813(2)	0.173(2)	0.013(2)
O3 (8f)	0.0001 CCD	0.2338(5)	0.3559(3)	0.1694(1)	0.0183(6)
	0.0001 PD	0.2341(5)	0.3566(3)	0.1693(1)	0.0179(6)
	P_0^a	0.239(3)	0.357(1)	0.169(1)	0.017(2)
	P_1	0.237(3)	0.355(1)	0.171(1)	0.013(2)
	P_2	0.243(3)	0.358(1)	0.173(1)	0.016(2)
	P_3	0.244(3)	0.359(1)	0.174(1)	0.015(2)
	P_4	0.240(3)	0.360(1)	0.173(1)	0.018(2)
	P_5^b	0.250(2)	0.360(1)	0.178(1)	0.013(2)
	P_6	0.249(2)	0.361(1)	0.178(1)	0.018(2)
	P_7	0.249(2)	0.365(1)	0.179(1)	0.018(2)
	P_8	0.251(3)	0.360(2)	0.180(2)	0.010(2)
	P_9	0.254(3)	0.363(2)	0.180(2)	0.013(2)
	P_{10}	0.252(3)	0.359(2)	0.183(2)	0.013(2)
O4 (8f)	0.0001 CCD	0.4569(5)	0.9382(3)	0.0544(1)	0.0164(5)
	0.0001 PD	0.4565(5)	0.9385(3)	0.0542(1)	0.0143(6)
	P_0^a	0.464(3)	0.940(2)	0.055(1)	0.017(2)
	P_1	0.460(3)	0.937(2)	0.055(1)	0.013(2)
	P_2	0.453(3)	0.938(1)	0.054(1)	0.016(2)
	P_3	0.456(3)	0.935(2)	0.054(1)	0.015(2)
	P_4	0.456(3)	0.935(2)	0.054(1)	0.018(2)
	P_5^b	0.452(3)	0.933(1)	0.055(1)	0.013(2)
	P_6	0.450(2)	0.933(2)	0.055(1)	0.018(2)
	P_7	0.454(3)	0.933(2)	0.055(1)	0.018(2)
	P_8	0.460(4)	0.931(2)	0.055(2)	0.010(2)
	P_9	0.452(3)	0.933(2)	0.057(2)	0.013(2)
	P_{10}	0.455(4)	0.931(2)	0.054(2)	0.013(2)

Table 2 continued

Sites	P (GPa)	x	y	z	$Uiso, Ueq$
O5 (8f)	0.0001 CCD	0.3952(5)	0.2515(3)	0.0544(1)	0.0152(5)
	0.0001 PD	0.3949(5)	0.2518(3)	0.0543(1)	0.0141(6)
	P_0^a	0.392(2)	0.253(2)	0.053(1)	0.017(2)
	P_1	0.393(3)	0.252(2)	0.056(1)	0.013(2)
	P_2	0.397(2)	0.253(2)	0.054(1)	0.016(2)
	P_3	0.395(2)	0.250(2)	0.055(1)	0.015(2)
	P_4	0.398(2)	0.249(1)	0.054(1)	0.018(2)
	P_5^b	0.401(2)	0.251(2)	0.054(1)	0.013(2)
	P_6	0.401(2)	0.250(2)	0.055(1)	0.018(2)
	P_7	0.404(2)	0.251(2)	0.055(1)	0.018(2)
	P_8	0.403(3)	0.251(2)	0.058(1)	0.010(2)
	P_9	0.401(3)	0.248(2)	0.056(1)	0.013(2)
	P_{10}	0.401(3)	0.249(3)	0.057(2)	0.013(2)
OH (8f)	0.0001 CCD	0.4546(5)	0.5652(3)	0.0529(1)	0.0192(6)
	0.0001 PD	0.4545(5)	0.5643(3)	0.0529(1)	0.0183(6)
	P_0^a	0.456(3)	0.566(2)	0.052(2)	0.017(2)
	P_1	0.451(3)	0.562(2)	0.054(2)	0.013(2)
	P_2	0.451(3)	0.568(2)	0.052(2)	0.016(2)
	P_3	0.455(3)	0.567(1)	0.053(2)	0.015(2)
	P_4	0.458(3)	0.567(1)	0.054(2)	0.018(2)
	P_5^b	0.452(3)	0.565(1)	0.052(2)	0.013(2)
	P_6	0.456(3)	0.568(2)	0.057(2)	0.018(2)
	P_7	0.450(3)	0.568(1)	0.055(2)	0.018(2)
	P_8	0.449(4)	0.564(2)	0.054(2)	0.010(2)
	P_9	0.451(4)	0.558(2)	0.050(3)	0.013(2)
	P_{10}	0.444(4)	0.561(2)	0.053(3)	0.013(2)

Anisotropic refinements have been performed only with the crystal in air (CCD data and PD data). The scattering curve of potassium alone was used for the K-site, and the refined electron content with the crystal in air was $18.2e^-$ (CDD data) and $18.4e^-$ (PD data), respectively. A mixed scattering curve with (Al + Fe, neutral) at the octahedral M-site was used, and the refined electron content per site with the crystal in air was $14.4e^-$ (CDD data) and $14.2e^-$ (PD data), respectively. For the T1 and T2 sites, the scattering curve of (neutral) Si was used, with refined electron content per site: $13.7e^-$ (CDD data) and $13.4e^-$ (PD data) at the T1, and $13.5e^-$ (CDD data) and $13.5e^-$ (PD data) at the T2, respectively. The structure refinements with the crystal in the DAC at any pressure were conducted with isotropic displacement factors by grouping all of the T-sites and all of the O-sites and with the occupancy of the K-, M-, T1- and T2-site fixed to the value refined with the crystal in air (PD-data). Standard errors, in units of the last decimal place, are given in parentheses.

[a] With the crystal in the DAC without P-medium

[b] With the crystal in decompression

the combination of the high compressibility of the inter-layer polyhedron with the moderate compressibility of the tetrahedral and octahedral sheets. The hydrostatic compression of the structure leads to a non-isotropic shortening of the K–O bond distances (Table 3, Figs. 1, 2), accompanied by an increase of the K-polyhedron distortion upon P (Table 3). The evolution of the volume of the inter-layer polyhedron with P shows a monotonically decreasing and smooth trend (Fig. 1). Fitting the P–V(K-polyhedron) data by a truncated II-BM-EoS, we obtain K_{T0}(K-polyhedron) = 26(1) GPa.

The octahedral-sheet is significantly less compressible than the inter-layer region. As shown in Fig. 3, the evolution of the volume of the occupied M-octahedron with P is monotonically decreasing within the P range investigated. A II-BM-EoS fit yields: K_{T0}(M-polyhedron) = 120(10) GPa.

The average bond-lengths and polyhedral volumes of the T1- and T2-sites do not show significant change with P (Table 3), though an inspection of the tetrahedral ξ-parameters of Table 3 reveals a significant increase of distortion. This suggests that the tetrahedra do tend to preserve their volume values as a function of pressure at the expense of their geometrical regularity, presumably to exploit a low-energy mechanism of compliance to P.

The anisotropic compression of the K-polyhedron is related to the main P-induced distortion affecting the tetrahedral sheet and occurring through a "ditrigonalization" of the six-membered rings of tetrahedra (6 mR), via a cooperative rotation of the polyhedra involved. Such a mechanism is described by the ditrigonal rotation angle [i.e. $\alpha = 1/6 \sum_{i=1}^{6} |120 - \varphi_i|/2$, where φ_i is the angle between basal edge of neighbouring tetrahedra articulated in the 6 mR, Brigatti and Guggenheim 2002], as a function of P (Figs. 4, 5). The α-parameter increases linearly with P up to 7–8 GPa, whereas for $P > 8$ GPa a "plateau" is observed, somehow suggesting the occurrence of a "saturation effect" (Fig. 5, Table 3). The volume of the K-polyhedron and the value of the α-rotation exhibit a high correlation (about 93%) up to 8 GPa (Fig. 6, Table 3).

The void volume, calculated as the difference between the unit-cell volume and the total of the volumes of the polyhedra, shows a trend with P, here not shown for the sake of brevity, fully similar to that of the ditrigonal distortion angle.

The structural relaxation corresponding to "corrugation" has a secondary importance with respect to that involving the ditrigonal rotation. The corrugation parameter (here not reported as immaterial to our discussion) did not show any regular trend as a function of P. We attribute that to the comparatively small portion of reciprocal space explored at HP conditions, which often makes it difficult to get insight into the most subtle structure rearrangements driven by P. Such interpretation is substantiated by the fact that a refinement of the structure at room conditions restricted only to the hkl-reflections accessible at HP fails to determine the correct corrugation parameter.

Discussion

This study follows our recent experiments on the high-pressure behaviour of a 3T-phengite, whose single-crystal structural data have been provided up to about 10 GPa (Gatta et al. 2009). Earlier experiments were, in fact,

Table 3 Relevant bond distances (Å), polyhedral volumes (Å^3), polyhedral distortion coefficients (ξ) and "ditrigonal rotation angle" (α, °) at different pressures

P (GPa)		0.0001 (P_0-AIR-PD)	0.0001[a] (P_0)	0.78(6) (P_1)	1.76(7) (P_2)	2.40(7) (P_3)	3.34(6) (P_4)	5.38(7) (P_5^b)	6.30(8) (P_6)	7.13(9) (P_7)	9.73(8) (P_8)	9.95(9) (P_9)	11.4(10) (P_{10})
T1	−O1	1.639 (3)	1.63 (1)	1.63 (1)	1.63 (1)	1.63 (1)	1.62 (1)	1.62 (1)	1.61 (1)	1.63 (1)	1.64 (2)	1.64 (2)	1.63 (2)
	−O2	1.633 (3)	1.64 (1)	1.64 (1)	1.64 (1)	1.63 (1)	1.62 (1)	1.61 (1)	1.63 (1)	1.61 (1)	1.63 (2)	1.62 (2)	1.60 (2)
	−O3	1.638 (3)	1.64 (1)	1.65 (1)	1.64 (2)	1.66 (2)	1.63 (2)	1.65 (1)	1.64 (1)	1.64 (1)	1.66 (2)	1.65 (2)	1.66 (2)
	−O4	1.622 (3)	1.62 (2)	1.62 (2)	1.63 (2)	1.64 (2)	1.63 (2)	1.63 (2)	1.64 (2)	1.61 (2)	1.63 (2)	1.62 (2)	1.64 (2)
<T1–O>		1.633	1.63	1.64	1.63	1.64	1.62	1.63	1.63	1.63	1.64	1.63	1.63
V(T1)		2.23(2)	2.23(6)	2.24(7)	2.24(7)	2.25(7)	2.20(6)	2.22(6)	2.22(7)	2.20(6)	2.24(8)	2.21(8)	2.22(9)
ξ (T1)		0.0026	0.0025	0.0030	0.0029	0.0036	0.0056	0.0038	0.0044	0.0035	0.0091	0.0064	0.0119
T2	−O1	1.639 (3)	1.63 (1)	1.64 (1)	1.64 (1)	1.65 (1)	1.64 (1)	1.63 (1)	1.63 (1)	1.63 (1)	1.64 (2)	1.63 (2)	1.63 (2)
	−O2	1.631 (3)	1.63 (1)	1.61 (1)	1.62 (1)	1.62 (1)	1.64 (1)	1.62 (1)	1.61 (1)	1.61 (1)	1.61 (2)	1.64 (2)	1.63 (2)
	−O3	1.641 (3)	1.63 (1)	1.62 (1)	1.63 (1)	1.63 (1)	1.62 (1)	1.62 (1)	1.61 (1)	1.64 (1)	1.59 (2)	1.61 (2)	1.61 (2)
	−O5	1.621 (3)	1.63 (2)	1.62 (2)	1.61 (2)	1.62 (2)	1.65 (2)	1.64 (2)	1.64 (2)	1.63 (2)	1.62 (2)	1.64 (2)	1.62 (2)
<T2–O>		1.633	1.63	1.62	1.63	1.63	1.64	1.63	1.62	1.63	1.61	1.63	1.62
V(T2)		2.22(1)	2.22(6)	2.20(7)	2.20(6)	2.21(6)	2.24(6)	2.20(6)	2.20(7)	2.21(6)	2.15(7)	2.16(8)	2.18(9)
ξ (T2)		0.0023	0.0054	0.0026	0.0036	0.0040	0.0044	0.0056	0.0048	0.0050	0.0066	0.0082	0.0079
α		5.48(9)	5.6(6)	5.6(6)	6.8(6)	6.9(5)	7.7(6)	8.8(6)	9.1(5)	10.1(5)	9.6(7)	10.6(8)	9.9(8)
M	–O4	1.954 (3)	1.99 (2)	1.98 (2)	1.95 (2)	1.95 (2)	1.89 (2)	1.94 (2)	1.92 (2)	1.94 (2)	1.96 (2)	1.92 (2)	1.94 (2)
	–O4′	1.985 (3)	1.96 (2)	1.96 (2)	1.98 (2)	1.96 (2)	1.99 (2)	1.96 (2)	1.96 (2)	1.96 (2)	1.87 (2)	1.94 (2)	1.89 (3)
	−O5	1.988 (3)	1.99 (2)	2.00 (2)	1.97 (2)	1.96 (2)	1.91 (2)	1.96 (2)	1.93 (2)	1.95 (2)	1.97 (2)	1.93 (2)	1.96 (3)
	–O5′	1.953 (3)	1.92 (2)	1.94 (2)	1.92 (2)	1.95 (2)	1.97 (2)	1.91 (2)	1.94 (2)	1.92 (2)	1.92 (2)	1.94 (3)	1.91 (3)
	–O6	1.949 (3)	1.94 (3)	1.98 (3)	1.94 (3)	1.92 (2)	1.90 (2)	1.89 (2)	1.92 (2)	1.92 (2)	1.92 (3)	1.86 (3)	1.93 (4)
	–O6′	1.939 (3)	1.94 (2)	1.91 (2)	1.93 (2)	1.94 (2)	1.98 (3)	1.88 (2)	1.95 (2)	1.90 (2)	1.85 (3)	1.79 (3)	1.79 (4)
<M–O>		1.961	1.96	1.96	1.95	1.94	1.94	1.92	1.94	1.93	1.92	1.90	1.90
V(M)		9.89(3)	9.8(2)	9.9(2)	9.7(2)	9.6(2)	9.6(2)	9.3(2)	9.5(2)	9.4(2)	9.2(2)	9.0(2)	8.9(3)
ξ (M)		0.0175	0.0193	0.0173	0.0179	0.0180	0.0179	0.0197	0.0153	0.0158	0.0180	0.0230	0.0205
K	–O1 (×2)	2.966 (3)	2.98 (1)	2.93 (1)	2.88 (1)	2.86 (1)	2.83 (1)	2.74 (1)	2.75 (1)	2.69 (1)	2.63 (2)	2.62 (2)	2.59 (2)
	–O1′ (×2)	3.166 (3)	3.15 (2)	3.14 (2)	3.15 (2)	3.12 (2)	3.14 (2)	3.14 (1)	3.13 (2)	3.13 (1)	3.08 (2)	3.10 (2)	3.09 (2)
	–O2 (×2)	3.315 (3)	3.32 (2)	3.29 (2)	3.27 (2)	3.27 (2)	3.27 (2)	3.26 (2)	3.24 (2)	3.28 (2)	3.15 (2)	3.17 (2)	3.17 (3)
	–O2′ (×2)	2.996 (3)	2.97 (2)	2.96 (2)	2.92 (2)	2.90 (2)	2.82 (2)	2.79 (2)	2.76 (2)	2.74 (2)	2.67 (2)	2.62 (2)	2.65 (3)
	–O3 (×2)	3.174 (3)	3.18 (2)	3.14 (2)	3.15 (2)	3.14 (2)	3.13 (2)	3.09 (2)	3.10 (2)	3.10 (2)	3.06 (2)	3.07 (2)	3.01 (3)
	–O3′ (×2)	2.959 (3)	2.95 (2)	2.93 (2)	2.86 (2)	2.84 (2)	2.84 (2)	2.75 (2)	2.73 (2)	2.69 (2)	2.67 (2)	2.64 (2)	2.65 (2)
<K–O>		3.096	3.09	3.06	3.04	3.02	3.00	2.962	2.950	2.94	2.88	2.87	2.86
V(K)		62.3(2)	61.8(9)	60.3(10)	58.9(9)	57.9(10)	56.5(9)	54.7(9)	53.5(9)	53.5(9)	48.4(10)	48.0(11)	47.9 (12)
ξ (K)		0.1730	0.1757	0.1741	0.1725	0.1724	0.1775	0.1698	0.1758	0.1664	0.1977	0.1991	0.1911

Standard errors, in units of the last decimal place, are given in parentheses. A few are given to two places to avoid misunderstanding

ξ is the polyhedral distortion coefficient calculated using the IVTON package (Balic-Zunic and Vickovic 1996; Makovicky and Balic-Zunic 1998); $\alpha\,(°) = 1/6 \cdot \sum_{i=1}^{6} |120° - \varphi_i|/2$, where φ_i is the angle between basal edge of neighbouring tetrahedra articulated in the 6 mR (Brigatti and Guggenheim 2002)

[a] With crystal in the DAC without P-medium

[b] With the crystal in decompression

limited to describe the bulk compression behaviour (providing isothermal EoS) and the HP-stability of 2M_1- and 3T-phengites (Pavese et al. 1999; Smyth et al. 2000; Curetti et al. 2006).

Our structure refinements of the 2M_1-phengite show that, under hydrostatic pressure, the structure rearranges producing an anisotropic strain through the inter-layer site,

with the shortest K–O bond-distances being more compressible than the longest ones. A similar finding was observed also in 3T-phengite (Gatta et al. 2009) and in muscovite (Comodi and Zanazzi 1995). The bulk-modulus of the K-polyhedron in 2M_1-phengite [i.e. K_{T0}(K-polyhedron) = 26(1) GPa] is smaller that those found in muscovite [i.e. K_{T0}(K-polyhedron) = 33 GPa] and in 3T-phengite
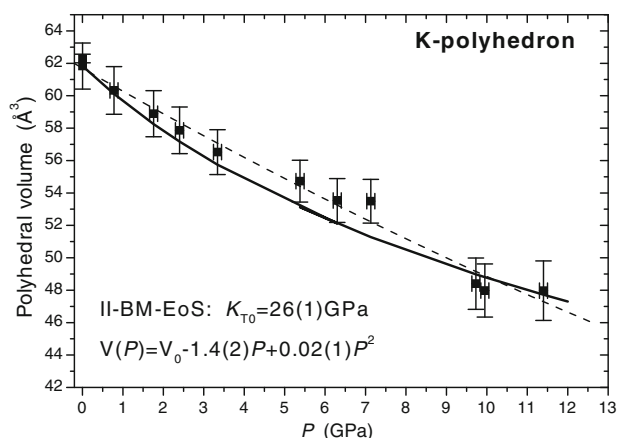
Fig. 1 Evolution of the inter-layers K-polyhedral volume with P. The *solid line* represents the second-order BM-EoS fit [with refined $K_{T0} = 26(1)$ GPa], whereas the *dotted line* represents the weighted polynomial fit [i.e. $V(P) = V_0 - 1.4(2)P + 0.02(1)P^2$] through the data points
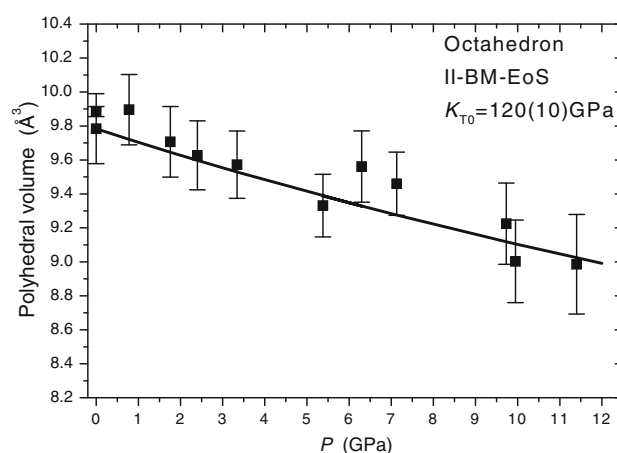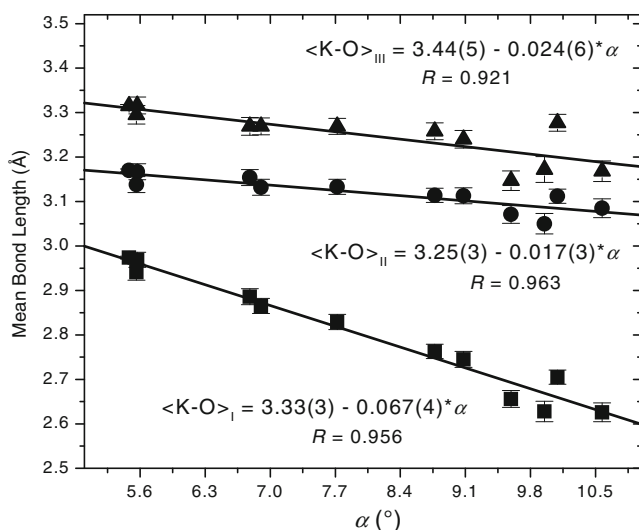

Fig. 3 Evolution of the octahedral volumes with P. The *solid lines* represent the II-BM-EoS fit through the data points

[i.e. K_{T0}(K-polyhedron) = 35(3) GPa, Gatta et al. 2009]; the latter two, in turn, are very similar to one another. The bulk-modulus of the octahedron in $2M_1$-phengite, i.e. $K_{T0} = 120(10)$ GPa, is close to that found for muscovite, i.e. 115 GPa, by Comodi and Zanazzi (1995).

As already observed in 3T-phengite (Gatta et al. 2009) and in other dioctahedral micas (Comodi and Zanazzi 1995; Zanazzi and Pavese 2002, and references therein), the relevant compressibility of the structure along [001] is mainly due to the compression of the K–O bond-distances, because of the comparatively weak cation–oxygen bonds of the inter-layer with respect to the M–O and T–O ones. The anisotropic compression mechanism of the inter-layer

polyhedron leads to a significant shortening of the bond distances between potassium and the basal oxygens of the tetrahedral sheet. The potassium–oxygen distance shortening takes place at different rates (Comodi and Zanazzi 1995; Zanazzi and Pavese 2002, and references therein; Comodi et al. 2004) as a function of the K–O bond lengths (Fig. 2); this is in keeping with an increase of the ditrigonal distortion of the 6 mR (Fig. 5), with $\partial\alpha/\partial P \approx 0.7°$/GPa between 0.0001 and 7–8 GPa, i.e. in the pressure range preceding the "saturation" plateau. The ditrigonal distortion is probably the most energy-convenient mechanism to make octahedral- and tetrahedral-sheets match one another so as to form the T–O–T layer (or T–M–T). Note that several studies show that an increase of the ditrigonal rotation favours the trigonal anti-prismatic (ideal

Fig. 2 Evolution of the K–O bond distances with P and with the ditrigonal rotation angle (α) (Table 3). The bond lengths are gathered in three groups: $\langle K–O\rangle_{III} = 1/2\cdot(2\cdot K\text{-}O2)$; $\langle K–O\rangle_{II} = 1/4\cdot(2\cdot K\text{-}O1'$

+ $2\cdot K\text{-}O3)$; $\langle K–O\rangle_I = 1/6\cdot(2\cdot K\text{-}O1 + 2\cdot K\text{-}O2' + 2\cdot K\text{-}O3')$; the *solid lines* represent the weighted linear regression through the data points
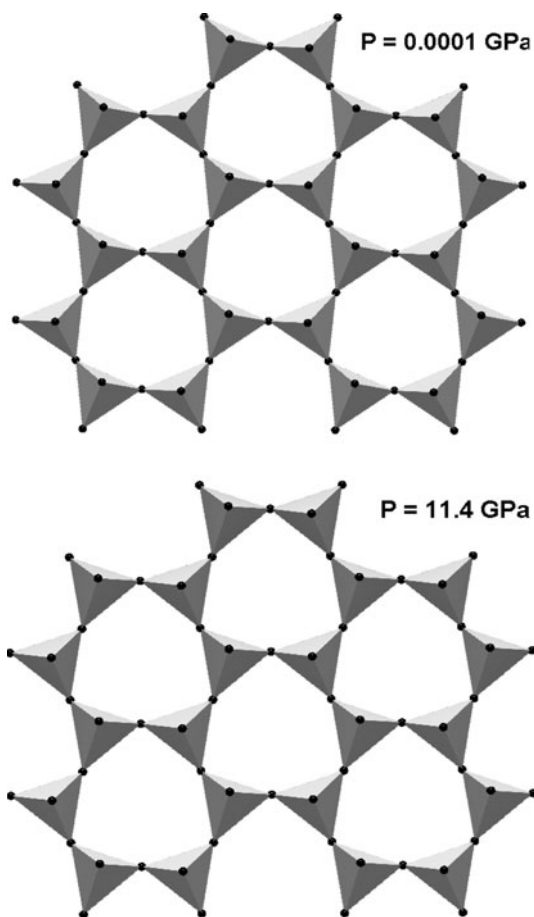
Fig. 4 Configuration of the six-membered rings of the tetrahedral sheet based on the structural refinements at 0.0001 and 11.4 GPa
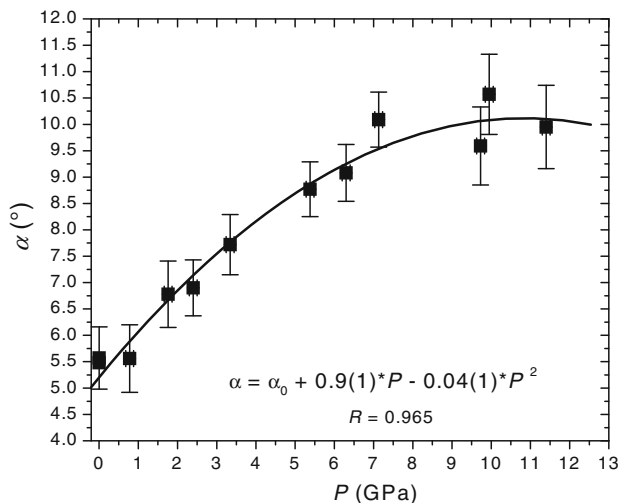

Fig. 5 Evolution of the "ditrigonal rotation angle", α, with P. The *solid curve* represents the weighted polynomial regression through all the data points
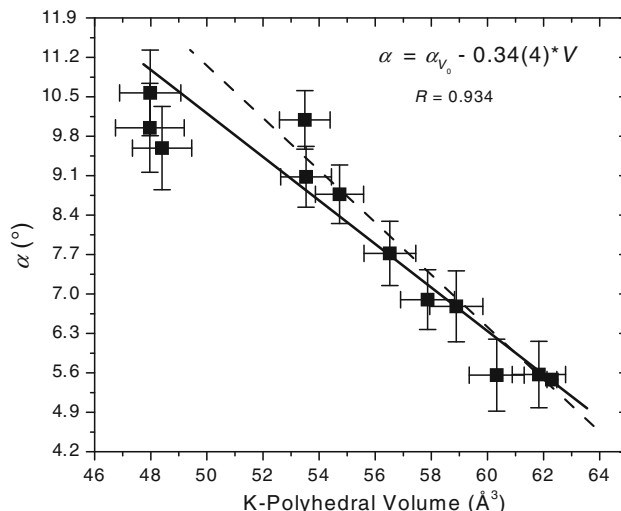

Fig. 6 Correlation between the "ditrigonal rotation angle", α, and the inter-layers K-polyhedral volume. The *solid line* represents the weighted linear regression through all the data points [*i.e.* 0.0001-11.4 GPa, with: $\alpha = \alpha_{V0} - 0.34(4)V$], whereas the *dotted line* represents the weighted linear regression through the data points between 0.0001 and 8 GPa

octahedral) coordination in the M-sheet; this is supposed to act as a possible stabilization factor of the structure (Ferraris and Ivaldi 2002). Conversely, an increase of

temperature is followed by a decrease of α, leading to a regularization of the 6 mR configuration (Ferraris and Ivaldi 2002; Zanazzi and Pavese 2002; Gemmi et al. 2008; Gatta et al. 2009).

The "saturation" effect observed in the evolution of α versus P at $P > 7$–8 GPa might mean that either

a. The structure is going to adopt a new mechanism of compliance to P in the tetrahedral sheet. However, our structure refinements at high-pressure did not reveal any hint of possible replacement of the ditrigonal distortion. Note that a slow transformation kinetic might hinder the rise of a new structure arrangement; or

b. the internal strain increases more and more portending a structure collapse, as suggested by the data collected above 15–17 GPa by Curetti et al. (2006).

Comparing the P-induced structure evolution of $2M_1$ to $3T$'s (Gatta et al. 2009), we observed that (1) similar anisotropic compression mechanisms of the inter-layer polyhedron occur in both polytypes, though the K_{T0} (K-polyhedron) value of $2M_1$ is about 30% smaller than that in $3T$; (2) the octahedra behave like quasi-rigid units in the trigonal polytype; in contrast, in the monoclinic mica an apparent compression occurs; (3) the tetrahedra behave like quasi-rigid units in both polytypes, though they are affected by larger distortions in $2M_1$- than in $3T$-phengite; (4) in both polytypes, correlations between the volume of the K-polyhedron, the volume of voids and the ditrigonal distortion angle (α) are observable; (5) the evolution of α versus P follows a linear trend in the $3T$-phengite over

the entire P range investigated; in contrast, in the $2M_1$-polytype a linear trend holds up to 7 GPa, and beyond a "saturation" plateau appears.

Let us now discuss the stability of monoclinic versus trigonal phengite polytypes in view of the polyhedral volume-pressure curves made available from the HP single-crystal structure refinements. The deformation energy as a function of P controls the stability of one polytype with respect to the other, and results in

$$G(P)_{\text{deform}} = \int_0^P V \mathrm{d}P$$

where 0 stands for room pressure and V is the molar volume; the integration is carried out along the isotherm at room temperature. If one expresses the cell volume in terms of its contributions due coordination polyhedra and voids, then $G(P)_{\text{deform}}$ can be recast as:

$$G(P)_{\text{deform}} = \sum_{j=1}^n \int_0^P V_{\text{polyhedral,j}} \mathrm{d}P + \int_0^P V_{\text{void}} \mathrm{d}P$$

where j spans the polyhedra (inter-layer, octahedra and tetrahedra). Such a reformulation of $G(P)_{\text{deform}}$ highlights the contributes due to each structural unit to the total deformation energy, as shown by Fig. 7 reporting:

$$\Delta G(P)_{\text{deform}} = G(P)_{\text{deform},3T} - G(P)_{\text{deform},2M1}.$$

In the moderate pressure regime, up to 7–8 GPa, $3T$ and $2M_1$ exhibit a total $\Delta G(P)_{\text{deform}}$-curve oscillating around zero, which does not allow to assert one polytype to be more stable than the other. A significant turn occurs beyond 7–8 GPa, owing to a change of the void-involving
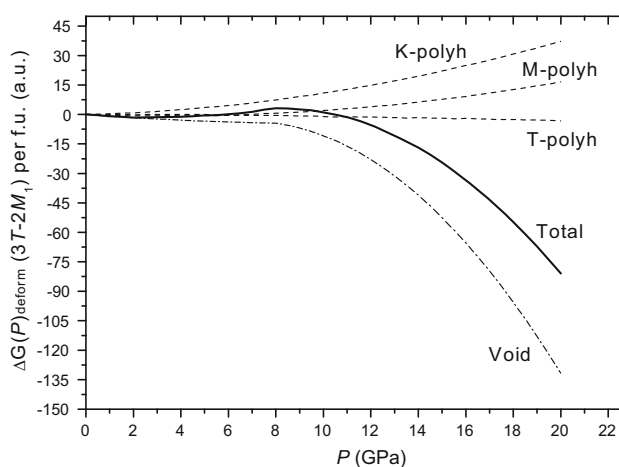
compression mechanism that leads to an apparent improvement of stability for $3T$. All this takes place along with the occurrence of the lock-up of the ditrigonal distortion angle in the monoclinic polytype. Under the circumstances, the structural relaxation operated through a cooperative polyhedral rearrangement via ditrigonal rotation at the expense of voids seems to be a reasonable candidate to explain the structure mechanism of V-compression favouring, in terms of deformation energy, the $3T$ polytype. Such a polytype can exploit a "more adjustable" octahedral sheet (with two symmetry independent sites) than $2M_1$'s (one symmetry independent site), thus allowing "less constrained" α-rotations of the Si/Al-tetrahedral rings to better fit the T- and O-modules into a compressed T–O–T layer, whose lattice parameters a and b shorten, with respect to an ideal structure, in terms of $a \times \cos(\alpha)$ and $b \times \cos(\alpha)$, respectively.

The mechanism we have discussed above relies upon polyhedral $V(P)$-curves affected by uncertainties, due to (a) the intrinsic difficulty to extract precise structural information from HP single-crystal data collections (b) the comparatively moderate P range explored and (c) the approximation used to model the volume–pressure relationships. Although we expect the compressibility of a solid to be better determined by measuring the unit-cell volume as a function of P ($K_{T0} \sim 57$ GPa, for $2M_1$) than reconstructing the compressibility via the polyhedral elastic behaviour ($K_{T0} \sim 52$ GPa, for $2M_1$; in this case, tetrahedra have been considered as infinitely rigid); however, the latter provides a way to interpret the microscopic mechanism underlying the macroscopic phenomena under pressure. Under the circumstances, we are confident that our modeling, though presumably somewhat poor of precision and overestimating the void-contribution, provides a comparatively correct depiction of the different structure responses of the two phengite polytypes to pressure and a reasonable structure interpretation of the better stability of $3T$ at HP than $2M_1$, as also indicated by petrologic data and reasoning (Sassi et al. 2009, and references therein).

Fig. 7 Difference deformation energy between $3T$ and $2M_1$ (given in arbitrary units, a.u.) versus P. Contributions due to inter-layer polyhedron (*dashed line*), octahedra (*dashed line*), tetrahedra (*dashed line*) and voids (*dot-dashed line*). The *solid curve* corresponds to the total difference deformation energy function

References

Angel RJ (2000) Equation of state. In: Hazen RM, Downs RT (eds) High-temperature and high-pressure crystal chemistry. Reviews in mineralogy and geochemistry, vol 41. Mineralogical Society of America and Geochemical Society, Washington, DC, pp 35–59

Angel RJ (2002) Absorb v5.2. Computer program. Crystallography laboratory. Department Geological Sciences, Virginia Tech, Blacksburg, USA. http://www.crystal.vt.edu

Angel RJ (2003) Automated profile analysis for single-crystal diffraction data. J Appl Cryst 36:295–300

Angel RJ, Bujak M, Zhao J, Gatta GD, Jacobsen SD (2007) Effective hydrostatic limits of pressure media for high-pressure crystallographic studies. J Appl Crystallogr 40:26–32

Balic-Zunic T, Vickovic I (1996) IVTON (Version 2)—program for the calculation of geometrical aspects of crystal structures and some crystal chemical applications. J Appl Crystallogr 29:305–306

Brigatti MF, Guggenheim S (2002) Mica crystal chemistry and the influence of pressure, temperature, and solid solution on atomistic models. In: Mottana A, Sassi FP, Thompson JB Jr, Guggenheim S (eds) Micas: crystal chemistry and metamorphic petrology. Review in mineralogy and geochemistry, vol 46. Mineralogical Society of America and Geochemical Society, Washington, DC, pp 1–97

Burnham CW (1966) Computation of absorption correction and the significance of end effect. Am Mineral 51:159–167

Catti M, Ferraris G, Hull S, Pavese A (1994) Powder neutron diffraction study of $2M_1$ muscovite at room pressure and at 2 GPa. Eur J Mineral 6:171–178

Comodi P, Zanazzi PF (1995) High-pressure structural study of muscovite. Phys Chem Minerals 22:170–177

Comodi P, Zanazzi PF (1997) Pressure dependence of structural parameters of paragonite. Phys Chem Minerals 24:274–280

Comodi P, Fumagalli P, Montagnoli M, Zanazzi PF (2004) A single-crystal study on the pressure behavior of phlogopite and petrological implications. Am Mineral 89:647–653

Compagnoni R (1977) The Sesia–Lanzo Zone: high pressure low temperature metamorphism in the Austroalpine continental margin. Rend Soc It Min Petr 23:335–374

Curetti N, Levy D, Pavese A, Ivaldi G (2006) Elastic properties and stability of coexisting $3T$ and $2M_1$ phengite polytypes. Phys Chem Minerals 32:670–678

Curetti N, Ferraris G, Ivaldi G (2008) Correlation between crystallization pressure and structural parameters of phengites. Am Mineral 93:451–455

Faust J, Knittle E (1994) The equation of state, amorphization, and high-pressure phase diagram of muscovite. J Geophys Res 99:19785–19792

Ferraris G, Ivaldi G (2002) Structural features of micas. In: Mottana A, Sassi FP, Thompson JB Jr, Guggenheim S (eds) Micas: crystal chemistry and metamorphic petrology. Review in mineralogy and geochemistry, vol 46. Mineralogical Society of America and Geochemical Society, Washington, DC, pp 117–53

Gatta GD, Rotiroti N, Pavese A, Lotti P, Curetti N (2009) Structural evolution of a $3T$ phengite mica up to 10 GPa: an in situ single-crystal X-ray diffraction study. Z Kristallogr 224:302–310

Gemmi M, Merlini M, Pavese A, Curetti N (2008) Thermal expansion and dehydroxylation of phengite micas. Phys Chem Minerals 35:367–379

Guidotti CV, Sassi FP (1998) Petrogenetic significance of Na–K white mica mineralogy: recent advances for metamorphic rocks. Eur J Mineral 10:815–854

Guidotti CV, Sassi FP (2002) Constraints on studies of metamorphic K–Na white micas. In: Mottana A, Sassi FP, Thompson JB Jr, Guggenheim S (eds) Micas: crystal chemistry and metamorphic petrology. Review in mineralogy and geochemistry, vol 46. Mineralogical Society of America and Geochemical Society, Washington, DC, pp 413–448

Ivaldi G, Ferraris G, Curetti N, Compagnoni R (2001) Coexisting $3T$ and $2M_1$ polytypes of phengite from Cima Pal (Val Savenca, Western Alps): chemical and polytypic zoning and structural characterization. Eur J Mineral 13:1025–1034

Kisch HJ, Sassi R, Sassi FP (2006) The b_0 lattice parameter and chemistry of phengites from HP/LT metapelites. Eur J Mineral 18:207–222

Makovicky E, Balic-Zunic T (1998) New measure of distortion for coordination polyhedra. Acta Crystallogr B54:766–773

Miletich R, Allan DR, Kuhs WF (2000) High-pressure single-crystal techniques. In: Hazen RM, Downs RT (eds) High-temperature and high-pressure crystal chemistry. Reviews in mineralogy and geochemistry, vol 41. Mineralogical Society of America and Geochemical Society, Washington, DC, pp 445–519

Nespolo M, Ďurovič S (2002) Crystallographic basis of polytypism and twinning in micas. In: Mottana A, Sassi FP, Thompson JB Jr, Guggenheim S (eds) Micas: crystal chemistry and metamorphic petrology. Review in mineralogy and geochemistry, vol 46. Mineralogical Society of America and Geochemical Society, Washington, DC, pp 155–279

Nespolo M, Ferraris G (2001) Effects of the stacking faults on the calculated electron density of mica polytypes—the Ďurovič effect. Eur J Mineral 13:1035–1045

Nespolo M, Ďurovič S (2002) Crystallographic basis of polytypism and twinning in micas. In: Mottana A, Sassi FP, Thompson JB Jr, Guggenheim S (eds) Micas: crystal chemistry and metamorphic petrology. Review in mineralogy and geochemistry, vol 46. Mineralogical Society of America and Geochemical Society, Washington, DC, pp 155–279

Oxford Diffraction (2008) Oxford Diffraction Ltd, Xcalibur CCD system, CrysAlis Software system

Pavese A, Ferraris G, Pischedda V, Mezouar M (1999) Synchrotron powder diffraction study of phengite $3T$ from the Dora–Maira massif: P–V–T equation of state and petrological consequences. Phys Chem Minerals 26:460–467

Rieder M, Cavazzini G, YuS D'Yakonov, Frank-Kamenetskii VA, Gottardi G, Guggenheim S, Koval PV, Mueller G, Neiva AMR, Radoslovich EW, Robert JL, Sassi FP, Takeda H, Weiss Z, Wones DR (1999) Nomenclature of the micas. Min Mag 63:267–279

Sassi FP, Guidotti CV, Rieder M, De Pieri R (1994) On the occurrence of metamorphic $2M_1$ pengites: some thoughts onpolytypism and crystallization conditions of $3T$ phengites. Eur J Mineral 6:151–160

Sassi R, Brigatti MF, Gomez-Pugnaire MT, Peruzzo L, Tellini F, Sassi FP (2009) What drives the distribution in nature of $3T$ vs. $2M_1$ polytype in muscovites and phengites? A general assessment based on new data from metamorphic and igneous granitoid rocks. In: Proceeding of "Geoitalia 2009", Rimini (Italy). Epitome, 17

Sekine T, Rubin AM, Ahrens TJ (1991) Shock wave equation of state of muscovite. J Geophys Res 96:19675–19680

Sheldrick GM (1997) SHELX-97. Programs for crystal structure determination and refinement. University of Göttingen, Germany

Smyth JR, Jacobsen SD, Swope RJ, Angel RJ, Arlt T, Domanik K, Holloway JR (2000) Crystal structures and compressibilities of synthetic $2M_1$ and $3T$ phengite micas. Eur J Mineral 12:955–963

Vaughan MT, Guggenheim S (1986) Elasticity in muscovite and its relationship to crystal structure. J Geophys Res 91:4657–4664

Wilson AJC, Prince E (1999) International tables for X-ray crystallography, vol C. Mathematical, physical and chemical tables, 2nd edn, Kluwer, Dordrecht

Zanazzi PF, Pavese A (2002) Behavior of micas at high pressure and high temperature. In: Mottana A, Sassi FP, Thompson JB Jr, Guggenheim S (eds) Micas: crystal chemistry and metamorphic petrology. Review in mineralogy and geochemistry, vol 46. Mineralogical Society of America and Geochemical Society, Washington, DC, pp 99–116